WAVELENGTH-SELECTIVITY

Maximizing the performance of photothermal actuators by combining smart materials with supplementary advantages

Tongyu Wang,[1] David Torres,[1] Félix E. Fernández,[2] Chuan Wang,[1] Nelson Sepúlveda[1]*

The search for higher-performance photothermal microactuators has typically involved unavoidable trade-offs that hinder the demonstration of ubiquitous devices with high energy density, speed, flexibility, efficiency, sensitivity, and multifunctionality. Improving some of these parameters often implies deterioration of others. Photothermal actuators are driven by the conversion of absorbed optical energy into thermal energy, which, by different mechanisms, can produce mechanical displacement of a structure. We present a device that has been strategically designed to show high performance in every metric and respond to optical radiation of selected wavelength bands. The device combines the large energy densities and sensitivity of vanadium dioxide (VO_2)–based actuators with the wavelength-selective absorption properties of single-walled carbon nanotube (SWNT) films of different chiralities. SWNT coatings increased the speed of VO_2 actuators by a factor of 2 while decreasing the power consumption by approximately 50%. Devices coated with metallic SWNT were found to be 1.57 times more responsive to red light than to near-infrared, whereas semiconducting SWNT coatings resulted in 1.42 times higher responsivities to near-infrared light than to red light. The added functionality establishes a link between optical and mechanical domains of high-performance photoactuators and enables the future development of mechanical logic gates and electronic devices that are triggered by optical radiation from different frequency bands.

INTRODUCTION

The performance of photoactuators that use optical energy to induce mechanical motion in micrometer-sized devices has improved significantly with the incorporation of novel photosensitive materials. Recent efforts include photoactuators based on polymers (*1*–*4*), oxides (*5*–*7*), hydrogels (*8*–*10*), graphenes (*11*–*13*), and single-walled carbon nanotubes (SWNTs) (*14*, *15*), which exhibit promising performance for applications such as remote controls, motors, switches, artificial muscles, and solar energy harvesters. The most developed actuation mechanism principles are photochemical (*16*–*18*) and photothermal (*14*, *19*–*21*) effects. For example, light radiation has been used to drive photochemical reactions in chromophores such as azobenzenes (*16*, *17*, *22*–*24*), which exhibit reversible response with visible and ultraviolet light illumination. However, the response time for typical photochemical actuators is in the order of seconds. By using photothermal actuation of polymer-based actuators (*11*, *25*, *26*), a bending angle of 70° is achieved with an exposure time of about 1 s. Although current technological trends in mechanical photoactuators are focused on using optical radiation intensity as the parameter used to characterize the response of the device, some reports have proposed the use of wavelength. Photoactuators using carbon nanotubes with selective chirality distributions have shown how the strong light absorption of SWNTs can be used to develop a sunlight-driven motor (*14*) and how the wavelength selectivity of gold nanocrystals can be used to develop photoactuators (*21*).

Despite the significant progress, the miniaturization of high-performance multifunctional photoactuators still represents a great challenge. Improving some performance metrics of micromechanical photoactuators (for example, energy density, multifunctionality, power consumption, speed, sensitivity, and fabrication complexity) often comes at the cost of worsening others. The reversible insulator-to-metal transition in VO_2, which has been known for almost 60 years (*27*), is accompanied by a structural transition (monoclinic to tetragonal). As was found much more recently (*28*), the resulting changes in mechanical stresses between a VO_2 film and a substrate generated by this reversible phase transition can be used to drive microactuators. In 2010, it was observed that when VO_2 film coatings on micromechanical structures go through the phase transition, which occurs in this material (triggered at a temperature of ~68°C), a substantial stress is generated, which produces large and reversible mechanical deflection (*28*). Later, VO_2-based photoactuators demonstrated response times in the order of milliseconds (*6*, *7*) and energy densities similar to those obtained using shape memory alloys (*29*, *30*). However, the large power consumption of VO_2-based photoactuators limited their scope of applications. On the other hand, photoactuators based on SWNTs have demonstrated high photothermal efficiency but with slow responses and low energy density. It was demonstrated that, by adding SWNT film coating as a light absorber, the photothermal efficiency of VO_2-based microphotoactuators can be improved (*20*). However, a single micromechanical photoactuator that combines large displacement, low power consumption, wavelength responsivity, fast actuation, high energy density, and compatibility with conventional microelectromechanical system (MEMS) fabrication processes has not been demonstrated.

Here, a design that uses the chirality-dependent optical properties of SWNTs is presented. The presented VO_2/SWNT-based micromechanical photoactuators show displacements that are dependent on the wavelength of the incident light on the device while maintaining excellent performance in terms of large displacement, low power consumption, large energy density, and fast response, which are the most important criteria in MEMS. For example, in remote control and switching applications of photoactuators, large displacement, low energy consumption, and fast response are critical, whereas in applications for motors and artificial muscles, energy density is of great importance. The most typical

[1]Department of Electrical and Computer Engineering, Michigan State University, East Lansing, MI 48824, USA. [2]Department of Physics, University of Puerto Rico-Mayagüez, Mayagüez, PR 00681, USA.
*Corresponding author. Email: nelsons@egr.msu.edu

technologies for photoactuators rely on the different thermal expansion coefficients of a bimorph structure and photochemical methods. However, maintaining high performance in all the metrics mentioned above for a single device is rather difficult. Thus, the present study breaks the common trade-offs that are typically needed to be carried out in a microactuator design, demonstrating an approach to optimize device performance while also adding wavelength-selective functionality. The developed device can find applications in soft microrobotics and monochromatic sensors, such as portable spectrometers, and can enable optically triggered microelectromechanical devices where MEMS-based logic gates, multiplexers, and decoders can be controlled by light pulses of different wavelengths.

RESULTS

Device fabrication

Figure 1A schematically illustrates the fabrication process of VO_2/SWNT actuators. The process starts with a 2-inch silicon wafer coated with 1-μm-thick silicon dioxide (SiO_2) layer deposited by plasma-enhanced chemical vapor deposition at 300°C. A thin layer of VO_2 (50 nm thick) was then deposited on a SiO_2 layer by pulsed laser deposition (PLD) (details in Materials and Methods). The quality of the VO_2 thin film was characterized by measuring its resistance as a function of temperature, which shows a resistance drop of nearly three orders of magnitude, as temperature changes from 30° to 100°C (see fig. S1), indicating a good-quality VO_2. The SWNT thin films tested in this study were made by vacuum filtration technique (details in Materials and Methods) using three different types of SWNT solutions shown in Fig. 1B. Unsorted SWNT (uSWNT), metallic SWNT (mSWNT), and semiconducting SWNT (sSWNT) are solutions containing a mixture of chiralities (*31*–*33*). These SWNT films were transferred on top of the VO_2/SiO_2-coated silicon wafers following a surface functionalization process similar to the one used by Wang *et al.* (*20*). The patterning of the SWNT and VO_2 films was carried out by oxygen plasma etching and SF_6-based reactive ion etching, respectively. The mechanical release of the cantilever structure was carried out by isotropic etching of the silicon substrate using XeF_2 gas. The cantilever structure of the photoactuators in this study is 400 μm long and 40 μm wide. Figure 1C shows the top view of the released photoactuators with different SWNT films, and Fig. 1D shows a cross-section scanning electron microscope (SEM) image of the device. The thickness of all the SWNT films was in the vicinity of 100 nm (see Materials and Methods).

Photothermal response

The SWNT films in the photoactuators serve as a light absorber layer, with the absorption spectrum dependent on its chirality distribution. Figure 2A shows the absorption spectra of the VO_2/uSWNT, VO_2/mSWNT, and VO_2/sSWNT films, indicating a near-flat spectrum for VO_2/uSWNT and spectra with peaks for VO_2/mSWNT and VO_2/sSWNT at approximately 700 and 1000 nm, respectively. Two semiconductor lasers with wavelengths of 660 and 985 nm are used in this study, which are absorbed better by the mSWNT and sSWNT films, respectively (see Fig. 2A). To make a fair comparison that demonstrates wavelength selectivity, the intensity of both lasers should be the same during the experiments. To this end, each laser was coupled into single-mode optical fibers, and a laser beam profiler was used to verify if the output of each fiber had the same Gaussian profile and a beam diameter of 500 μm (see fig. S2). The tested samples were mounted on a Peltier heater that maintained the sample's temperature at 40°C during laser illumination normal to the sample's substrate. This preheating to 40°C is required to photothermally increase the temperature of the devices completely across the phase transition with the lasers used. A charge-coupled device camera (resolution, 720 × 480) was used to monitor the deflection of the actuators. The details of the measurement setup are illustrated in fig. S3 and note S1.

Before performing the laser experiments, deflections of the four types of actuators were measured as functions of temperature to verify the phase transition characteristics of VO_2 after the whole fabrication process and to confirm that the structural phase transition of VO_2 is the dominating actuation mechanism. The results in Fig. 2B show the deflection of all the actuators as the temperature was varied across the phase transition of VO_2 (from 30° to 100°C). It can be seen that all types of actuators (that is, VO_2 and VO_2/SWNT actuators) show a similar shape for the abrupt hysteretic behavior during the heating-cooling cycle. This proves that the dominant actuation mechanism in the SWNT-coated actuator is the stress generated during the phase transition of VO_2 and suggests that the advantages of VO_2-based actuators (for example, large displacement and high energy density) are still present after SWNT coating.

Figure 2 (C to F) shows the photothermal response of VO_2 and VO_2/SWNT actuators as a function of laser power while the samples were kept at an initial temperature of 40°C. It can be noticed that, when the devices are actuated by conductive heating (Fig. 2B), the maximum deflection is larger than that of photothermal actuation (Fig. 2, C to F). This difference is due to the fact that part of the heat generated during photothermal actuation is dissipated by the temperature gradient between the device and the substrate, which is maintained at 40°C; this temperature gradient is much smaller for conductive heating. Once the substrate is brought to a given temperature by conductive heating, the bulk of the device acts as an infinite heat reservoir, making the heat loss through the suspended cantilever structure negligible and increasing the uniformity of the temperature in the structure.

The high absorption of SWNT films can be readily observed by comparing the results for the VO_2-based actuator (Fig. 2C) with any of the VO_2/SWNT-based actuators (Fig. 2, D to F). Regardless of the different response for the two tested wavelengths, all VO_2/SWNT actuators require less laser power to reach the phase transition; that is, they have a lower "triggering power" (P_T). It can be noticed that the VO_2-based actuator has a lower P_T for 660-nm laser illumination, but the rate of change in displacement per unit power (that is, responsivity) during the phase transition of VO_2 is lower for 660 nm. At low temperature, VO_2 films show higher optical absorption at 660 nm than at 985 nm, but the absorption spectrum of VO_2 changes during the transition, resulting in a higher optical absorption at 985 nm than at 660 nm (see fig. S4). This causes a crossover of the curves at a laser power of approximately 56 mW. On the other hand, the photothermal response of VO_2/SWNT actuators is mainly determined by the absorption properties of the SWNT film coating, which do not show variations with temperature changes across the phase transition of VO_2.

Wavelength-dependent response

Because of the flat absorption spectrum of the uSWNT film, the photothermal responses in VO_2/uSWNT for the 660- and 985-nm wavelengths are practically overlapping (see Fig. 2D). However, the VO_2/mSWNT and VO_2/sSWNT actuators show different responses for the two wavelengths used. It is clear that film absorption depends on the optical properties and thickness of the film. Therefore, although the absorption coefficient of the mSWNT and sSWNT films is wavelength-dependent,

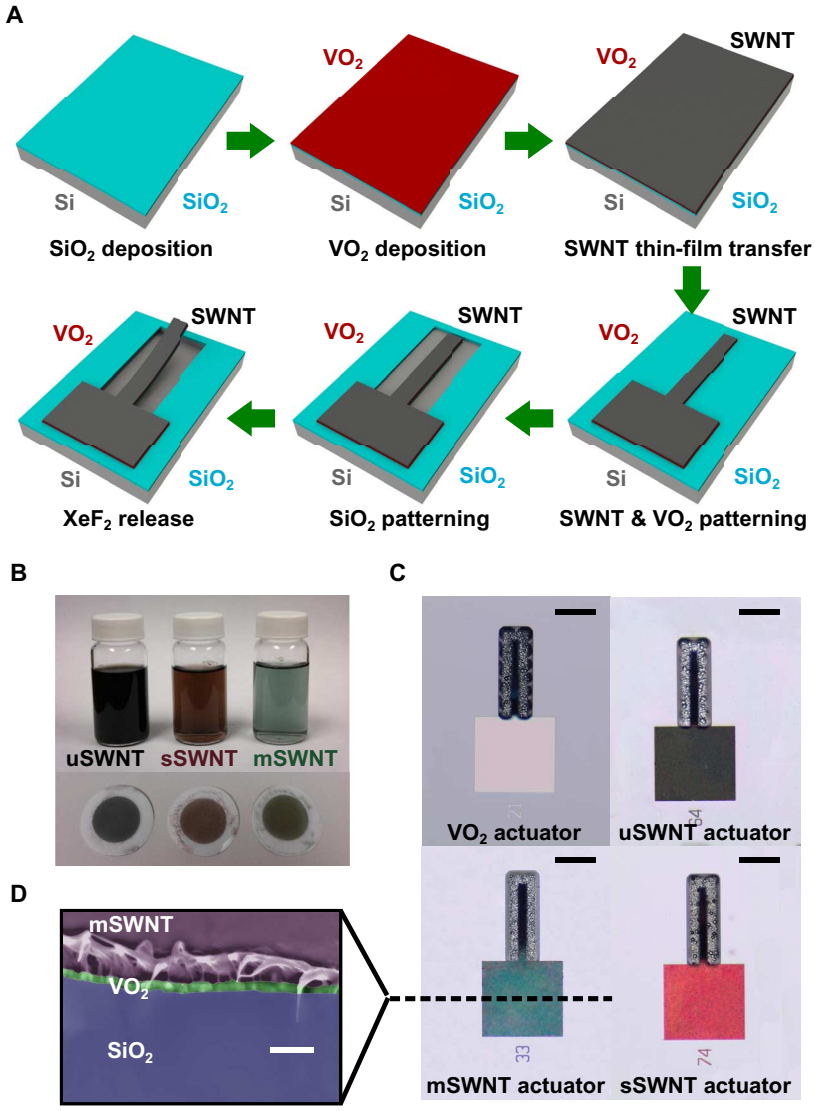

Fig. 1. Fabrication process of VO_2/SWNT microactuators. (**A**) Schematics illustrating the fabrication process of VO_2/SWNT microactuators. (**B**) Optical images of uSWNT, mSWNT, and sSWNT solution and SWNT/cellulose membranes made of SWNT solution by vacuum filtration. Scale bar, 20 mm. (**C**) Top-view microscope images of bare VO_2, VO_2/uSWNT, VO_2/mSWNT, and VO_2/sSWNT microactuators. All the cantilevers had the same length and width of 400 and 40 μm, respectively. Scale bars, 200 μm. (**D**) SEM image of a cross section of the VO_2/mSWNT actuators. Colors have been artificially modified for clarity. Scale bar, 200 nm.

this property can be masked by a large thickness (see note S2 for details). We found that a thickness of 100 nm was enough to maintain a continuous SWNT film with wavelength-dependent absorption spectrum. To study the wavelength-selective response of VO_2/mSWNT-based actuators, we tested both wavelengths on the same device so that differences in response are not caused by differences in film thickness of either mSWNT or VO_2. Furthermore, by comparing the responses of a device with a given initial deflection, we have the same illuminated surface area and consequently the same delivered power for both wavelengths.

The separations between photothermal response curves in Fig. 2 (E and F) are attributed to the wavelength-dependent absorption coefficients of the mSWNT and sSWNT films. Because of the optical absorption peak around 700 nm for the mSWNT films (and all other parameters being equal) (see Fig. 2A), the temperature increase for mSWNT will be higher for illumination from the 660-nm laser. Thus, the VO_2/mSWNT actuators will have a lower P_T for illumination from the 660-nm laser (see Fig. 2E). Conversely, the sSWNT films have better absorption for 985 nm, which translates into a lower P_T for illumination from the 985-nm laser (see Fig. 2F). Furthermore, the responsivity across the phase transition is higher for 660-nm illumination in the VO_2/mSWNT actuator and for 985-nm illumination in the VO_2/sSWNT actuator. Therefore, energy from light is being absorbed and converted to heat more efficiently for the wavelength of higher absorption across the entire phase transition range of VO_2. Table 1 summarizes the responsivity between wavelengths for all the SWNT-coated devices.

The wavelength-selective response of the present devices is better visualized in Fig. 3 and in the movies presented in the Supplementary Materials (description of the movies is in note S3). A laser power of 30 mW was used for both lasers (660 and 985 nm), as labeled in Fig. 2 (C to F). This power is much lower than the P_T for the bare VO_2–based microactuator, and therefore, the device shows negative displacements (that is, displacements toward the substrate) for both wavelengths

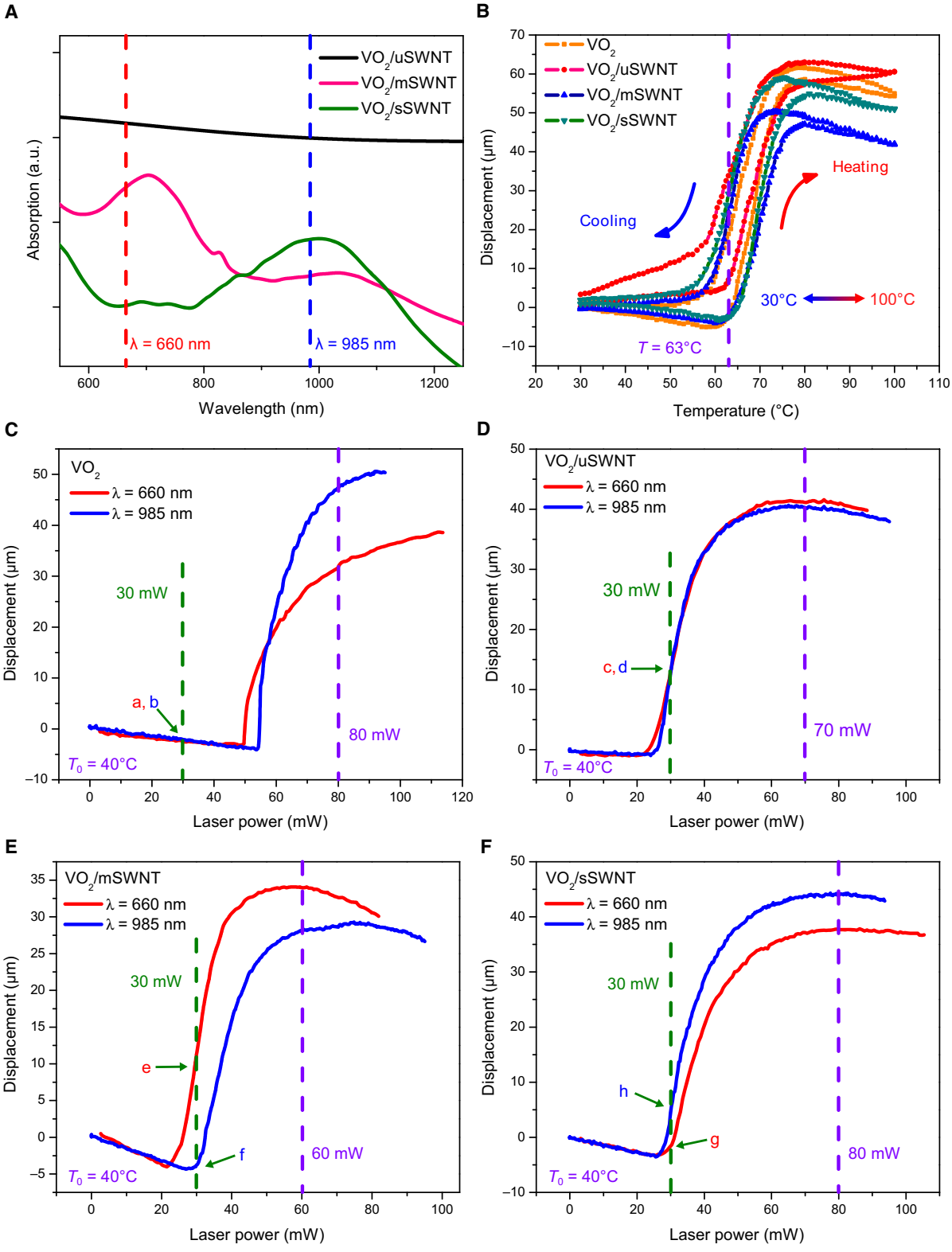

Fig. 2. Photothermal response of VO_2/SWNT microactuators. (**A**) Measured optical absorption spectra of VO_2/uSWNT, VO_2/mSWNT, and VO_2/sSWNT films, which are composed of a 50-nm-thick VO_2 and a 100-nm-thick SWNT film. The two wavelengths (660 and 985 nm) used in this study are marked in the plot. a.u., arbitrary units. (**B**) Measured displacement of all types of actuators as a function of temperature. A Peltier heater in contact with the bottom of the silicon substrate was controlled to cycle the temperature from 30° to 100°C. Measured displacements as functions of laser power (660 and 985 nm) of (**C**) bare VO_2, (**D**) VO_2/uSWNT, (**E**) VO_2/mSWNT, and (**F**) VO_2/sSWNT actuators while the substrate temperature was set to 40°C. The laser power used in time response measurements is marked by purple dashed lines, whereas the laser power used for wavelength-selective actuation is marked by green dashed lines. The measured points (a, b, c, d, e, f, g, and h) correspond to Fig. 3 (A to H).

(Fig. 3, A and B), which is induced by the mismatch between thermal expansion coefficient of VO_2 and SiO_2. Note that the VO_2 thin film has a higher thermal expansion coefficient than SiO_2. In contrast, VO_2/SWNT actuators have much higher photothermal efficiency than bare VO_2–based actuators. The VO_2/uSWNT actuator shows very similar displacement for both wavelengths (Fig. 3, C and D), which is consistent with the absorption spectrum shown in Fig. 2A. VO_2/mSWNT actuators are more responsive to 660-nm illumination and therefore show a larger deflection (almost fourfold) for this wavelength (Fig. 3, E and F). On the other hand, VO_2/sSWNT actuators show larger deflections for the 985-nm laser. The still images in Fig. 3 (G and H) (and the movies in the Supplementary Materials) show how a laser power of 30 mW for both laser wavelengths generates displacements in opposite directions for the VO_2/mSWNT-based and VO_2/sSWNT-based actuators.

Table 1. Light responsivity during phase transition. The responsivity is calculated from an estimate of the slope of displacement versus light power curve for the linear region across the phase transition in Fig. 2.

λ (nm)	Responsivity (μm/mW)		
	VO_2/uSWNT	VO_2/mSWNT	VO_2/sSWNT
660	2.74	3.13	2.48
985	2.74	2.00	3.51

Time response

For most conventional thermal microactuators, the actuation mechanism is based on thermal expansion of materials. The total displacement of actuators operated on this principle is proportional to the product of the difference in thermal expansion coefficient of the materials involved ($\Delta\alpha$) and the temperature change (ΔT). Because the $\Delta\alpha$ is inherently limited to values lower than 2×10^{-5} K^{-1} for metal-ceramic bimorphs (*34*) and to values in the vicinity of 2×10^{-4} K^{-1} for polymer-silicon bimorphs (*25*), the needed ΔT to generate large deflections is relatively high. Moreover, a larger ΔT requirement typically results in slower devices (*35*, *36*). Large displacements often require very large temperature changes (ΔT) and are therefore slow (*35*, *36*). In contrast, VO_2-based actuators rely on the material's phase transition, which happens at about 68°C and typically spans over a temperature window of only 5° to 10°C. Because of the lower ΔT required for full actuation, VO_2-based actuator devices are much faster than the similar designs based on thermal expansion mechanisms. Here, the time response of all types of actuators was captured by a high-speed camera (1200 frames/s), and the deflection is plotted as a function of time for pulses of different illumination powers from both lasers (see Fig. 4). Before actuation, the samples were preheated to 40°C. The laser pulse duration in all the plots is 25 ms, and the power used is marked in Fig. 2 (C to F). It should be noted that the laser power used for the time response experiments for the three different SWNT films [purple vertical dashed lines in Fig. 2 (D to F) and labeled power in Fig. 4 (A to D)] is different. This is carried out to be able to calculate the time response of each device. Each type of SWNT

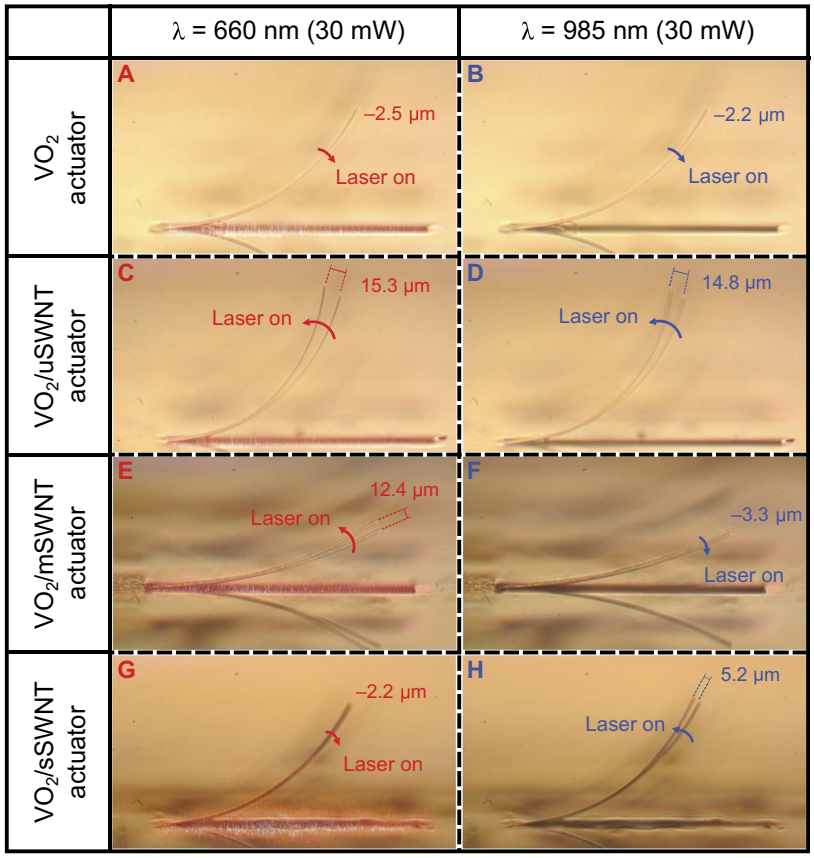

Fig. 3. Wavelength-selective actuation. (**A** to **H**) Light response of the four different actuators for pulses from both lasers (660 and 985 nm). For each wavelength, the power was calibrated to maintain the same delivered power of 30 mW that is marked in Fig. 2 with green dashed lines while the substrate temperature is maintained constant at 40°C.

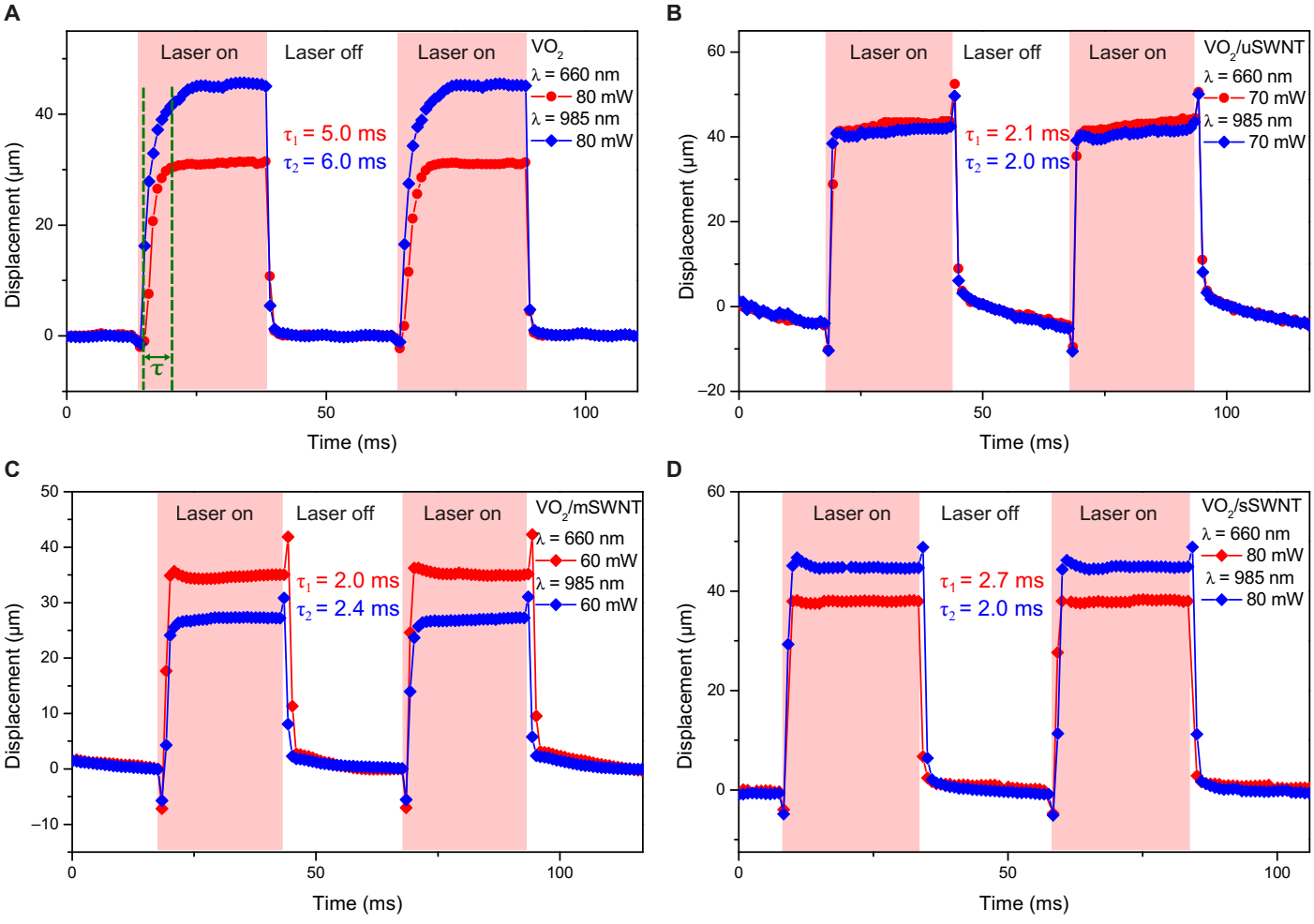

Fig. 4. Time response of VO_2/SWNT actuators. Measured displacements of (**A**) bare VO_2, (**B**) VO_2/uSWNT, (**C**) VO_2/mSWNT, and (**D**) VO_2/sSWNT actuators as lasers are turned on and off by controlling the driven current. The pulse duration is 25 ms for all tests. The power used in time response is also marked with purple dashed lines in Fig. 2. The response times show that VO_2/SWNT-based actuators are much faster than the uncoated device and that the wavelength-selective actuators respond faster to the better-absorbed wavelength.

film absorbs each wavelength differently. Therefore, the required amount of power to completely go through the transition region and achieve full actuation will be different for each type of SWNT film. Because the response time is the required time to achieve full actuation, it was necessary to use the power that resulted in full actuation for each device. The bare VO_2 actuator was not fully driven across the phase transition because of the power limitations of the lasers used. The response time is calculated as the time required for the displacement to rise from 10 to 90% of the stable value. All the VO_2/SWNT-based actuators are approximately twice as fast as the uncoated VO_2–based actuator. Furthermore, when comparing the time responses for the VO_2/mSWNT and VO_2/sSWNT, it is observed that each device responds faster to the wavelength that is better absorbed by the corresponding SWNT film.

It should be noted that the photothermal process is slower than the mechanical actuation process, which means that the time response of the photoactuators presented here will be ultimately limited by the speed with which the absorbed power is converted to heat and not by the mechanical properties of the device. This is expected because heat transfer in solids is, in general, much slower than the speed of sound in the material. A model that allows for estimating the time response is discussed in the Supplementary Materials.

Photothermal actuation mechanism

To better understand the actuation mechanism during photothermal actuation, a finite element method (FEM) model was created using COMSOL (version 4.4) software. Details on the simulation and model are found in note S4. Figure 5A illustrates the simulated surface temperature distribution of the VO_2/uSWNT actuator preheated to 40°C for a laser illumination of 30 mW. The temperature gradient along the cantilever's length, which was previously mentioned to be the main reason for the difference in largest deflections between photothermal and conductive heating actuation methods, is evident from the surface temperature profile shown in Fig. 5 (A and B). The simulated temperature profile as a function of cantilever length for different power values from the 660-nm laser for all the VO_2/SWNT-based actuators is shown in Fig. 5B. The energy dissipation due to convection losses is higher at the cantilever's tip. The temperature at 300 μm along the actuators as the function of 660-nm irradiation power is plotted in Fig. 5C.

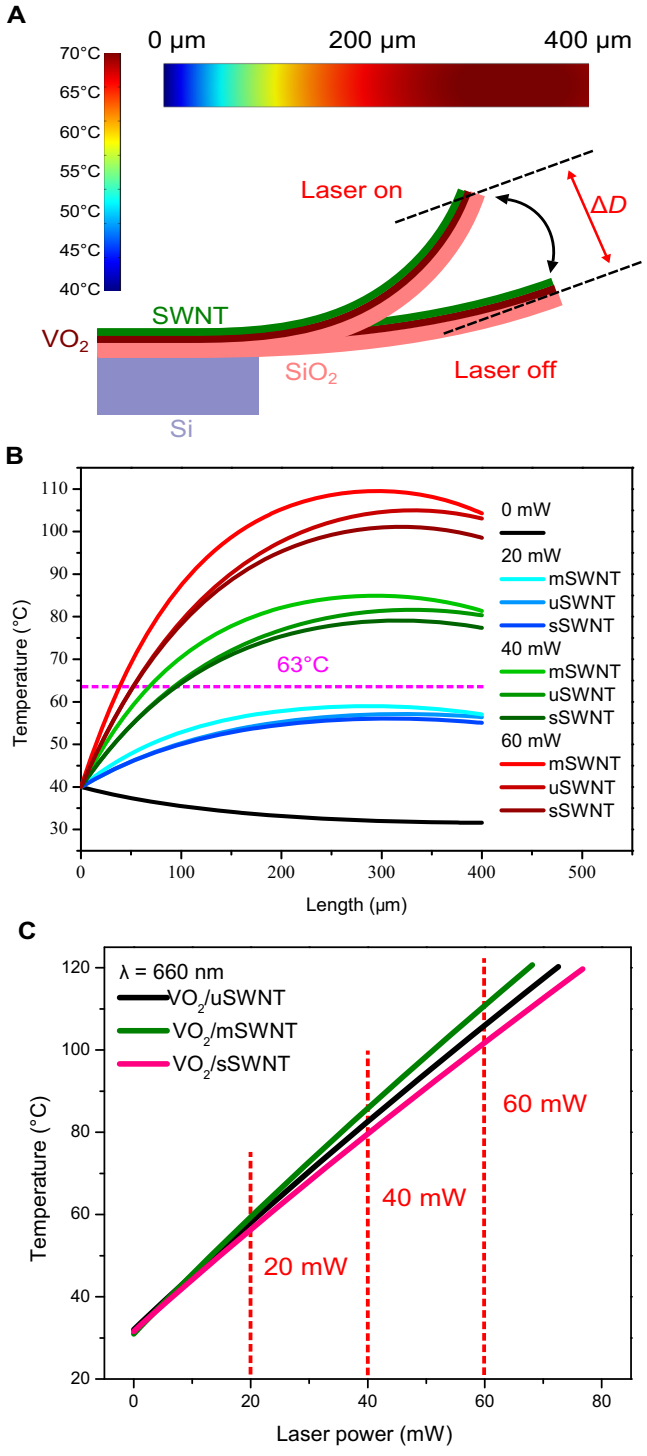

Fig. 5. Photothermal effects. (**A**) Schematic of the microactuator model used in the COMSOL simulation. When illuminated, the actuator is locally heated, resulting in the displacement of ΔD. Here, the anchor of the structure is fixed and maintained at a temperature of 40°C, same as the experiments. The inset shows the surface temperature distribution of VO_2/uSWNT actuator under the 660-nm laser illumination of 30 mW. (**B**) Calculated temperature distribution along the actuators' length (400 μm) under the 660-nm laser irradiation with different laser powers. The phase transition temperature of VO_2 is 63°C, marked by a purple dashed line. (**C**) Calculated temperature at the length of actuators (300 μm) as a function of laser power (660 nm). Purple dashed lines represent the power plotted in (B).

Simulations related to the dynamics of actuators were also carried out within the model. During the actuation, two processes contribute to the response time: (i) the conversion from optical energy to thermal energy and (ii) the conversion from thermal energy to mechanical energy. The first process can be described in Eq. 1

$$\rho C_p \frac{\partial T}{\partial t} = \nabla \cdot (k \nabla T) + Q \quad (1)$$

where ρ is the density of the structural materials, C_p is the specific heat, T is temperature, t is time, k is thermal conductivity, and Q contains all heat source and dissipation. The convective cooling of air and light illumination was introduced by a module in COMSOL software (see note S4). The thermal response time of the VO_2/uSWNT, VO_2/mSWNT, and VO_2/sSWNT actuators under a 40-mW laser irradiation was calculated to be 2.65, 3.0, and 2.82 ms, respectively, using COMSOL (see fig. S5). The time constant of the second process can be characterized by calculating the resonance frequencies of the structure. Given the geometry and mechanical properties of materials, the first resonance frequency of VO_2/uSWNT actuators is about 6 kHz. For an underdamped system, the rise time τ, which, by definition, is the response time in this paper, is estimated to be 0.16 ms < τ < 0.6 ms (see note S4). Therefore, the response time for the photothermal model is much larger than the mechanical time response, indicating that the conversion of optical energy into heat is the mechanism that determines the time response of the whole system. The measured response time for the present devices is similar to the one obtained from the photothermal model. The details about the simulation can be seen in note S4.

DISCUSSION

In summary, the present study demonstrates wavelength-selective VO_2/SWNT photothermal microactuators that combine the high performance of VO_2-based actuators with the excellent optical properties of SWNT, resulting in energy-efficient microdevices with high speed, large deflections, and wavelength-dependent response multifunctionality. The device fabrication is compatible with standard MEMS fabrication technologies, and the properties of the VO_2 or SWNT films are maintained in the process. This allows for the integration of the present devices into larger MEMS transducers or systems that involve components defined by conventional microlithography. The present device can find applications in monochromatic sensors such as portable spectrometers and can enable optically triggered microelectromechanical devices where MEMS-based logic gates, multiplexers, and decoders can be controlled by light pulses. Furthermore, the present study suggests that the response of VO_2-based photosensors or bolometers, which are very sensitive because of the large change in the resistance of VO_2 with temperature, can be made wavelength-dependent by using the SWNT film coatings. The measurements reported in this study could be extended to include more wavelengths by using single-chirality SWNT films with sharper absorption peaks than the mSWNT and sSWNT films.

MATERIALS AND METHODS

VO_2 deposition

The VO_2 thin film was deposited through PLD on substrates coated with a 1-μm-thick SiO_2 layer. The substrate was placed into a vacuum chamber with oxygen environment (15 mtorr). Facing the substrate, a metallic vanadium target, 2 inches apart from the substrate, was ablated

by excimer laser pulses with an intensity of 352 mJ (fluence, ~2 J/cm^2) and a frequency of 10 Hz. During the 10-min deposition, a ceramic heater was used to heat the sample and maintain its temperature at 595°C. After the deposition, a 30-min annealing process was performed under the same deposition conditions. To determine the quality of the VO_2 film, the resistance of the VO_2 film was measured as a function of temperature, which cycled from 30° to 100°C. A resistance drop close to three orders was observed during the cycle (see fig. S1).

SWNT film fabrication and transfer

All SWNT films used in this study were prepared by vacuum filtration. The mSWNT and sSWNT solutions with a purity of 95% (diameter, 1.2 to 1.7 nm) and a concentration of 0.01 mg/ml were bought from NanoIntegris, and the uSWNT solution (0.01 mg/ml) was made following, in general, the same processes of Zhang *et al.* (*14*). Purified SWNT powder (purity, >99 weight %; diameter, 0.8 to 1.6 nm; length, 3 to 30 μm) purchased from Cheap Tubes Inc. was mixed with 2% sodium deoxycholate as surfactant. An overnight sonication was performed to completely dissolve the SWNT powder. Then, centrifuging for 10 min with a rotation speed of 13,000 rpm helped remove large SWNT aggregates and non-SWNT impurities. The membranes used to filter the SWNT solution were cellulose membranes with a diameter of 2.5 mm, which were purchased from Millipore Inc. To achieve best filtration, membranes with different pore sizes are used to filtrate the mSWNT and sSWNT solutions (pore size, 0.025 μm) and the uSWNT solution (pore size, 0.45 μm). The thickness of SWNT films can be controlled by the amount of solution used for filtration. The relation between solution volume and film thickness is shown in fig. S6. Given the SWNT membrane made by vacuum filtration, acetone bath was used to transfer the SWNT film on a VO_2 surface wafer and remove the mixed cellulose membrane. To obtain good adhesion between SWNT and VO_2, surface functionalization was performed by immersing the target substrate into a poly-L-lysine solution for 5 min. Then, the cellulose/SWNT membrane was attached to VO_2 surface with the SWNT side facing toward the substrate. Several drops of deionized water were used to keep the membranes in the desired position. The substrate was placed upside down in a beaker, about 1 inch above the liquid acetone, on a hot plate that is set to 70°C. After about 1 hour of acetone vapor bath, cellulose membrane was dissolved, leaving only the SWNT film on the substrate. The transfer process was completed by briefly rinsing the sample with acetone and isopropanol and then by blow-drying the sample.

SUPPLEMENTARY MATERIALS

Supplementary material for this article is available at http://advances.sciencemag.org/cgi/content/full/3/4/e1602697/DC1

note S1. Photothermal response measurement.
note S2. Wavelength selectivity study for various SWNT film thickness.
note S3. Movie information.
note S4. Photothermal actuation model of VO_2/SWNT actuators.
note S5. Effects of different thermal conductivities and heat capacities between SWNT films.
note S6. Effects of SWNT film thickness in wavelength selectivity.
fig. S1. Resistance of VO_2 as a function of temperature.
fig. S2. Beam profiles for the lasers on the tested actuators.
fig. S3. Schematic of the setup used for photothermal and time response measurements.
fig. S4. Light absorption of the VO_2 thin film.
fig. S5. Simulated temperature change as a function of time.
fig. S6. The SWNT film thickness versus the volume of SWNT solution used for vacuum filtration.
fig. S7. Absorption spectra of sSWNT films for different thicknesses.
fig. S8. Photothermal response of SWNT films with different heat capacities.
fig. S9. Response time versus SWNT film thermal conductivity.
fig. S10. Wavelength selectivity as a function of thickness.
table S1. Material properties used in the FEM model.
movie S1. Wavelength-selective actuation of the VO_2 actuator.
movie S2. Wavelength-selective actuation of the VO_2/uSWNT actuator.
movie S3. Wavelength-selective actuation of the VO_2/mSWNT actuator.
movie S4. Wavelength-selective actuation of the VO_2/sSWNT actuator.
References (*37*–*39*)

REFERENCES AND NOTES

1. Y. Li, Y. He, X. Tong, X. Wang, Photoinduced deformation of amphiphilic azo polymer colloidal spheres. *J. Am. Chem. Soc.* **127**, 2402–2403 (2005).
2. A. Lendlein, S. Kelch, Shape-memory polymers. *Angew. Chem. Int. Ed.* **41**, 2034–2057 (2002).
3. M. A. C. Stuart, W. T. S. Huck, J. Genzer, M. Müller, C. Ober, M. Stamm, G. B. Sukhorukov, I. Szleifer, V. V. Tsukruk, M. Urban, F. Winnik, S. Zauscher, I. Luzinov, S. Minko, Emerging applications of stimuli-responsive polymer materials. *Nat. Mater.* **9**, 101–113 (2010).
4. K. Kumar, C. Knie, D. Bléger, M. A. Peletier, H. Friedrich, S. Hecht, D. J. Broer, M. G. Debije, A. P. H. J. Schenning, A chaotic self-oscillating sunlight-driven polymer actuator. *Nat. Commun.* **7**, 11975 (2016).
5. B. Kundys, M. Viret, D. Colson, D. O. Kundys, Light-induced size changes in $BiFeO_3$ crystals. *Nat. Mater.* **9**, 803–805 (2010).
6. R. Cabrera, E. Merced, N. Sepúlveda, F. E. Fernández, Dynamics of photothermally driven VO_2-coated microcantilevers. *J. Appl. Phys.* **110**, 094510 (2011).
7. E. Merced, N. Dávila, D. Torres, R. Cabrera, F. E. Fernández, N. Sepúlveda, Photothermal actuation of VO_2:Cr-coated microcantilevers in air and aqueous media. *Smart Mater. Struct.* **21**, 105009 (2012).
8. X. Zhang, C. L. Pint, M. H. Lee, B. E. Schubert, A. Jamshidi, K. Takei, H. Ko, A. Gillies, R. Bardhan, J. J. Urban, M. Wu, R. Fearing, A. Javey, Optically- and thermally-responsive programmable materials based on carbon nanotube-hydrogel polymer composites. *Nano Lett.* **11**, 3239–3244 (2011).
9. C. Yu, Z. Duan, P. Yuan, Y. Li, Y. Su, X. Zhang, Y. Pan, L. L. Dai, R. G. Nuzzo, Y. Huang, H. Jiang, J. A. Rogers, Electronically programmable, reversible shape change in two- and three-dimensional hydrogel structures. *Adv. Mater.* **25**, 1541–1546 (2013).
10. A. W. Hauser, A. A. Evans, J.-H. Na, R. C. Hayward, Photothermally reprogrammable buckling of nanocomposite gel sheets. *Angew. Chem. Int. Ed.* **54**, 5434–5437 (2015).
11. E. Wang, M. S. Desai, S.-W. Lee, Light-controlled graphene-elastin composite hydrogel actuators. *Nano Lett.* **13**, 2826–2830 (2013).
12. J. Liang, Y. Xu, Y. Huang, L. Zhang, Y. Wang, Y. Ma, F. Li, T. Guo, Y. Chen, Infrared-triggered actuators from graphene-based nanocomposites. *J. Phys. Chem. C* **113**, 9921–9927 (2009).
13. J. Loomis, X. Fan, F. Khosravi, P. Xu, M. Fletcher, R. W. Cohn, B. Panchapakesan, Graphene/elastomer composite-based photo-thermal nanopositioners. *Sci. Rep.* **3**, 1900 (2013).
14. X. Zhang, Z. Yu, C. Wang, D. Zarrouk, J.-W. T. Seo, J. C. Cheng, A. D. Buchan, K. Takei, Y. Zhao, J. W. Ager, J. Zhang, M. Hettick, M. C. Hersam, A. P. Pisano, R. S. Fearing, A. Javey, Photoactuators and motors based on carbon nanotubes with selective chirality distributions. *Nat. Commun.* **5**, 2983 (2014).
15. L. Chen, M. Weng, W. Zhang, Z. Zhou, Y. Zhou, D. Xia, J. Li, Z. Huang, C. Liu, S. Fan, Transparent actuators and robots based on single-layer superaligned carbon nanotube sheet and polymer composites. *Nanoscale* **8**, 6877–6883 (2016).
16. F. Terao, M. Morimoto, M. Irie, Light-driven molecular-crystal actuators: Rapid and reversible bending of rodlike mixed crystals of diarylethene derivatives. *Angew. Chem. Int. Ed.* **51**, 901–904 (2012).
17. Y. Takashima, S. Hatanaka, M. Otsubo, M. Nakahata, T. Kakuta, A. Hashidzume, H. Yamaguchi, A. Harada, Expansion–contraction of photoresponsive artificial muscle regulated by host–guest interactions. *Nat. Commun.* **3**, 1270 (2012).
18. S. Kobatake, S. Takami, H. Muto, T. Ishikawa, M. Irie, Rapid and reversible shape changes of molecular crystals on photoirradiation. *Nature* **446**, 778–781 (2007).
19. Z. Zhu, E. Senses, P. Akcora, S. A. Sukhishvili, Programmable light-controlled shape changes in layered polymer nanocomposites. *ACS Nano* **6**, 3152–3162 (2012).
20. T. Wang, D. Torres, F. E. Fernández, A. J. Green, C. Wang, N. Sepúlveda, Increasing efficiency, speed, and responsivity of vanadium dioxide based photothermally driven actuators using single-wall carbon nanotube thin-films. *ACS Nano* **9**, 4371–4378 (2015).
21. T. Lan, Y. Hu, G. Wu, X. Tao, W. Chen, Wavelength-selective and rebound-able bimorph photoactuator driven by a dynamic mass transport process. *J. Mater. Chem. C* **3**, 1888–1892 (2015).
22. E. Uchida, R. Azumi, Y. Norikane, Light-induced crawling of crystals on a glass surface. *Nat. Commun.* **6**, 7310 (2015).
23. Y. Yu, M. Nakano, T. Ikeda, Photomechanics: Directed bending of a polymer film by light. *Nature* **425**, 145 (2003).
24. H. Yu, T. Ikeda, Photocontrollable liquid-crystalline actuators. *Adv. Mater.* **23**, 2149–2180 (2011).

25. M. C. LeMieux, M. E. McConney, Y.-H. Lin, S. Singamaneni, H. Jiang, T. J. Bunning, V. V. Tsukruk, Polymeric nanolayers as actuators for ultrasensitive thermal bimorphs. *Nano Lett.* **6**, 730–734 (2006).
26. C. Jiang, M. E. McConney, S. Singamaneni, E. Merrick, Y. Chen, J. Zhao, L. Zhang, V. V. Tsukruk, Thermo-optical arrays of flexible nanoscale nanomembranes freely suspended over microfabricated cavities as IR microimagers. *Chem. Mater.* **18**, 2632–2634 (2006).
27. F. J. Morin, Oxides which show a metal-to-insulator transition at the Neel temperature. *Phys. Rev. Lett.* **3**, 34 (1959).
28. A. Rúa, F. E. Fernández, N. Sepúlveda, Bending in VO_2-coated microcantilevers suitable for thermally activated actuators. *J. Appl. Phys.* **107**, 074506 (2010).
29. E. Merced, X. Tan, N. Sepúlveda, Strain energy density of VO_2-based microactuators. *Sens. Actuators A* **196**, 30–37 (2013).
30. K. Liu, C. Cheng, Z. Cheng, K. Wang, R. Ramesh, J. Wu, Giant-amplitude, high-work density microactuators with phase transition activated nanolayer bimorphs. *Nano Lett.* **12**, 6302–6308 (2012).
31. S. Ghosh, S. M. Bachilo, R. B. Weisman, Advanced sorting of single-walled carbon nanotubes by nonlinear density-gradient ultracentrifugation. *Nat. Nanotechnol.* **5**, 443–450 (2010).
32. A. A. Green, M. C. Hersam, Nearly single-chirality single-walled carbon nanotubes produced via orthogonal iterative density gradient ultracentrifugation. *Adv. Mater.* **23**, 2185–2190 (2011).
33. X. Tu, S. Manohar, A. Jagota, M. Zheng, DNA sequence motifs for structure-specific recognition and separation of carbon nanotubes. *Nature* **460**, 250–253 (2009).
34. J. L. Corbeil, N. V. Lavrik, S. Rajic, P. G. Datskos, "Self-leveling" uncooled microcantilever thermal detector. *Appl. Phys. Lett.* **81**, 1306–1308 (2002).
35. L. Que, J.-S. Park, M.-H. Li, Y. B. Gianchandani, Reliability studies of bent-beam electro-thermal actuators, in *Proceedings of the 38th Annual 2000 IEEE International Reliability Physics Symposium*, San Jose, CA, 10 to 13 April 2000.
36. J. K. Luo, Y. Q. Fu, J. A. Williams, W. I. Milne, Thermal degradation of electroplated nickel thermal microactuators. *J. Microelectromech. Syst.* **18**, 1279–1287 (2009).
37. R. Cabrera, E. Merced, N. Sepúlveda, Performance of electro-thermally driven VO_2-based MEMS actuators. *J. Microelectromech. Syst.* **23**, 243–251 (2014).
38. W. S. Levine, *The Control Handbook: Control Systems Fundamentals* (CRC Press, ed. 2, 2011).
39. F. Lian, J. P. Llinas, Z. Li, D. Estrada, E. Pop, Thermal conductivity of chirality-sorted carbon nanotube networks. *Appl. Phys. Lett.* **108**, 103101 (2016).

Acknowledgments: We would like to thank J. Yeom for the helpful discussions regarding SWNT film transfer. **Funding:** This study was partially supported by the NSF Division of Electrical, Communications and Cyber Systems (ECCS) grant (ECCS 1306311). **Author contributions:** T.W. was in charge of the overall design of the devices, SWNT film transfers, and experiments. D.T. assisted with the VO_2 depositions and helped during the device fabrication. F.E.F. contributed to the theoretical modeling and analysis of the results. C.W. assisted with the design of the experiments and discussion of the results. N.S. assisted in the fabrication of the devices, analysis of the results, and preparation of the manuscript. All authors were included during the discussion of results and participated during the review of the manuscript. **Competing interests:** The authors declare that they have no competing interests. **Data and materials availability:** All data needed to evaluate the conclusions in the paper are present in the paper and/or the Supplementary Materials. Additional data related to this paper may be requested from the authors.

Submitted 3 November 2016
Accepted 23 February 2017
Published 21 April 2017
10.1126/sciadv.1602697

Citation: T. Wang, D. Torres, F. E. Fernández, C. Wang, N. Sepúlveda, Maximizing the performance of photothermal actuators by combining smart materials with supplementary advantages. *Sci. Adv.* **3**, e1602697 (2017).

Science Advances

Maximizing the performance of photothermal actuators by combining smart materials with supplementary advantages

Tongyu Wang, David Torres, Félix E. Fernández, Chuan Wang and Nelson Sepúlveda

Sci Adv **3** (4), e1602697.
DOI: 10.1126/sciadv.1602697

Science Advances (ISSN 2375-2548) is published by the American Association for the Advancement of Science, 1200 New York Avenue NW, Washington, DC 20005.